AGU PUBLICATIONS

JGR

Journal of Geophysical Research: Space Physics

RESEARCH ARTICLE
10.1002/2014JA020765

Key Points:
- Global observations of the solar wind including high-latitude regions
- Heliospheric response to long-term change in the solar dynamo activity
- Marked north-south asymmetry of the polar solar wind and its origin

Correspondence to:
M. Tokumaru,
tokumaru@stelab.nagoya-u.ac.jp

Citation:
Tokumaru, M., K. Fujiki, and T. Iju (2015), North-south asymmetry in global distribution of the solar wind speed during 1985–2013, *J. Geophys. Res. Space Physics*, *120*, 3283–3296, doi:10.1002/2014JA020765.

Received 27 OCT 2014
Accepted 12 MAR 2015
Accepted article online 16 MAR 2015
Published online 5 May 2015

North-south asymmetry in global distribution of the solar wind speed during 1985–2013

Munetoshi Tokumaru[1], Ken'ichi Fujiki[1], and Tomoya Iju[1]

[1]Solar-Terrestrial Environment Laboratory, Nagoya University, Nagoya, Japan

Abstract Interplanetary scintillation (IPS) observations made between 1985 and 2013 are used to investigate the north-south (N-S) asymmetry in global distribution of the solar wind speed. The IPS observations clearly demonstrate that the global distribution of the solar wind speed systematically changes with the solar activity. This change is found to closely correlate with that in polar magnetic fields of the Sun, while fast wind data at solar minima systematically deviate from this correlation. The IPS observations show that notable N-S asymmetry of polar solar winds occurs at the solar maxima, and small but significant N-S asymmetry exists at the solar minima. The observed asymmetry at the solar maxima is consistent with the time lag in the reversal of polar magnetic fields between north and south hemispheres. We also find that significant N-S asymmetry of the polar fast wind lasts for the period between Cycles 23 and 24 solar maxima, starting from predominance of the fast wind over the north pole and ending with that over the south pole. The N-S asymmetry revealed from IPS observations is found to be generally consistent with Ulysses observations. We compare IPS observations with magnetic field data of the Sun and find that the ratio of the quadrupole to dipole coefficients exhibits a similar time variation to that of the N-S asymmetry revealed from IPS observations. This suggests that higher-order multipole moments play an important role in determining the N-S asymmetry of the solar wind when the dipole moment weakens.

1. Introduction

The north-south (N-S) asymmetry of solar activity is considered as a basic feature of the dynamo process of the Sun [e.g., *Cowling*, 1933] and has been intensively investigated using various kinds of observed indicators [*Chowdhury et al.*, 2013, and references therein]. In contrast, the N-S asymmetry of the heliosphere, which is considered as a consequence of asymmetric solar activity, has been less studied owing to shortage of observational data with a global coverage. In an early time of in situ observations, i.e., before the Ulysses era, the displacement of the heliospheric current sheet (HCS) from the equator was deduced from width difference of IMF polarity sectors observed at the Earth's orbit [*Rosenberg*, 1975; *Tritakis*, 1984]. This displacement was ascribed to hemispheric difference in solar activity and solar wind pressure. The latitude offset of the HCS was evidently demonstrated from out-of-ecliptic in situ measurements by Ulysses [*Smith et al.*, 1997, 2000; *Virtanen and Mursla*, 2010; *Erdos and Balogh*, 2010]. Ulysses data showed that the magnitude of the high-latitude radial field of the southern hemisphere was larger than in the northern hemisphere during latitude scans for 1994–1995 and 2007 (solar minimum periods). In spite of its weaker magnetic flux, the northern polar coronal hole covered a larger area on the solar surface than the southern one [*Zhang et al.*, 2002], and this suggests that the HCS was shifted southward during these periods. Cosmic ray measurements by Ulysses also showed that the plane of symmetry was shifted southward from the heliographic equator during the fast latitude scan; 1994–1995 [*Simpson et al.*, 1996]. Such HCS displacements were identified for several intervals between 1976 and 2001 from the analysis of magnetograph observations at the Wilcox Solar Observatory, and they were found to be closely linked with the asymmetry in the characteristics of coronal holes between two hemispheres [*Zhao et al.*, 2005]. Hemispheric asymmetries in the properties of the solar wind and IMF originating from polar coronal holes were also investigated from Ulysses observations during the declining and minimum phase of Cycles 22 and 23, and significant N-S differences were found in several parameters [*McComas et al.*, 2000; *Ebert et al.*, 2013]. These differences were attributed to enhanced solar wind density and radial IMF in the southern hemisphere (40°–60°S), which may be closely linked to hemispheric asymmetries of the Sun's magnetic field and delay in evolution of the polar coronal hole [*Ebert et al.*, 2013].

For studying latitudinal asymmetry of the solar wind, remote sensing techniques are useful, since they enable us to make global observations in a short time (compared to the Ulysses orbital period). Space-borne observations of Lyman alpha heliospheric glow during 1996–2002 were used to investigate the N-S asymmetry of the solar wind [*Bzowski et al.*, 2003]. The Lyman alpha data during the solar minimum (1996–1998) demonstrated that the mass flux of the fast solar wind from the northern and southern polar coronal holes differed from each other and that the slow wind was offset slightly to the south with respect to the solar equator. Ground-based observations of interplanetary scintillation (IPS) also serve as a useful method for studying the global latitudinal structure of the solar wind [*Coles et al.*, 1980; *Kojima and Kakinuma*, 1990; *Manoharan*, 2012]. A small but significant N-S asymmetry, which is consistent with Ulysses observations, has been disclosed from the tomographic analysis of IPS observations in 1996 [*Kojima et al.*, 2001]. The different change in the distribution of fast solar wind at north and south polar regions has been reported from IPS observations in Cycle 24 [*Manoharan*, 2012].

In this study, we examine the N-S asymmetry of the solar wind speed distribution during 1985–2013; from the solar minimum between Cycles 22 and 23 to the solar maximum of Cycle 24. IPS observations, which have been collected since the 1980s using the multistation system [*Kojima and Kakinuma*, 1990], enable such a study covering over an unprecedentedly long period. The solar dynamo activity drastically declines during this period, and peculiar aspects of the solar wind have been reported at the extended solar minimum between Cycles 23 and 24 from some recent studies [*McComas et al.*, 2008, 2013; *Tokumaru et al.*, 2009, 2010, 2012; *Jian et al.*, 2011; *Manoharan*, 2012]. Therefore, long-term change of the N-S asymmetry for the period including Cycle 24 maximum is of great interest and provides improved understanding about the heliospheric response to the peculiar solar activity.

The outline of this paper is as follows. In section 2, we briefly describe Solar-Terrestrial Environment Laboratory (STEL) IPS observations and the analysis technique. In sections 3 and 4, we present long-term change in the global distribution of the solar wind speed and its N-S asymmetry during 1985 and 2013. Here we focus on the N-S asymmetry of polar solar winds, which are regarded as a key region for the solar dynamo activity. In section 5, we compare our IPS observations with Ulysses in situ measurements to examine the N-S asymmetry observed for polar solar winds. In section 6, we examine properties of the solar magnetic field as a cause for the N-S asymmetry of polar solar winds. In section 7, we summarize and discuss the results obtained here.

2. STEL IPS Observations

IPS observations at 327 MHz have been carried out regularly since 1983 at STEL using a multistation system, which consists of four radio telescopes at Toyokawa, Fuji, Kiso, and Sugadaira. [*Kojima and Kakinuma*, 1990; *Asai et al.*, 1995; *Tokumaru*, 2013]. Each radio telescope has a large aperture to achieve a high sensitivity which is essential for observing IPS. We collect IPS data for 30–40 sources on a daily basis between April and November/December using the multistation system. During winter, multistation IPS observations at STEL are unavailable owing to snowfall. In 2008, the IPS system at Toyokawa was upgraded to a more sensitive and reliable one, called the Solar Wind Imaging Facility (SWIFT) [*Tokumaru et al.*, 2011]. The SWIFT has a larger antenna aperture and a lower noise figure, which allow us to detect IPS for more sources of weak flux density (the minimum detectable flux density of the SWIFT is 0.2 Jy (jansky; 10–26 W m^{-2} Hz^{-1}) for an integration time of 100 ms, whereas that of the old system was 0.9 Jy), and no mechanical driving system, i.e., the antenna beam direction is controlled electronically, and this reduces an interruption rate due to problems of the driving system, resulting in improved reliability. The IPS systems at Fuji and Kiso was upgraded in 2010 in order to collect IPS data simultaneously with the SWIFT and to enable the cross-correlation analysis between those three stations. While either three or four radio telescopes are employed for multistation observations during the period analyzed here, we confirm that there exists no systematic bias between three- and four-station observations [*Tokumaru et al.*, 2010].

The solar wind speeds have been determined from the cross-correlation analysis of the multistation IPS data under an assumption of a solar wind flowing radially with a constant speed. The normalized scintillation level, called the *g* value, has been also determined since 1997 regularly from IPS data at one of STEL IPS stations [*Tokumaru et al.*, 2000]. In this study, we analyze these IPS data using the computer-assisted tomography (CAT) method to produce deconvolved maps of the solar wind speed on the source surface. In our analysis, the source surface is assumed to be located at 2.5 solar radii. The CAT method enables accurate

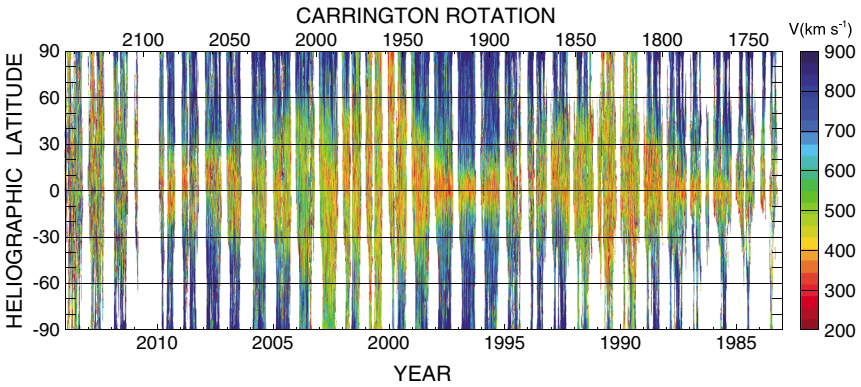

Figure 1. Synoptic source surface map of the solar wind speed derived from STEL IPS observations for the period from 1983 through 2013. Note that the time, i.e., the Carrington rotation number, increases from the right to the left in this figure. Red (blue) colors represent slow (fast) speeds.

determination of global distribution of the solar wind speed from IPS observations using multiple lines of sight [*Kojima et al.*, 1998; *Asai et al.*, 1998; *Jackson et al.*, 1998]. Among several versions of the CAT method developed so far, we employ here the time sequence CAT method, since it is suitable for studying in detail the quasi-stationary solar wind structure evolving with the solar activity [*Fujiki et al.*, 2003; *Kojima et al.*, 2007]. In deconvolving IPS data of solar wind speeds with any CAT methods, information on solar wind density fluctuations ΔN_e is required. We use g value data which represent the relative level of ΔN_e, when they are available, to deconvolve solar wind speed data, as in *Tokumaru et al.* [2012]. When the g value data are unavailable, i.e., before 1997, we assume an empirical relation between the solar wind speed V and ΔN_e as $\Delta N_e \propto V^{-0.5}$ as in *Tokumaru et al.* [2010]. Solar wind disturbances associated with fast coronal mass ejections do not follow this relation, but such short-lived effects are considered to be effectively eliminated through the model optimization process in the CAT method, where quasi-stationary structures persisting for a duration comparable to a solar rotation period are assumed.

3. Global Distribution of the Solar Wind Speed

The synoptic source surface map of the solar wind speed derived from STEL IPS observations between 1983 and 2013 is displayed in Figure 1. The horizontal and vertical axes are the time and heliographic latitude, respectively (Note that the time proceeds from the right to the left). The solar wind speed is indicated by color from red (slow) to blue (fast), and white areas denote the region where no IPS data are available. In addition to data gaps in every winter, there are several data gaps owing to system troubles or maintenance. For example, IPS data in 2010 are rather few owing to the system upgrade. Nevertheless, a long-term change in global distribution of the solar wind speed is evidently discernible from this figure. Our IPS observations demonstrate that fast solar winds develop over both north and south poles, particularly at around solar minima, while they disappear at solar maxima. In contrast, slow solar winds are located at the low-latitude region throughout the period analyzed here.

In order to discuss the long-term change quantitatively, we sort our IPS data into five groups by speed ranges; <445 km/s, 445–530 km/s, 530–615 km/s, 615–700 m/s, and >700 km/s and calculate fractional areas for the five speed groups to all observed areas in each year between 1985 and 2013. This method of data grouping has been used in our earlier studies [*Tokumaru et al.*, 2010, 2012]. Here we exclude IPS data obtained in 1983–1984 and 2010 owing to the small number of data for those years. The calculated fractional areas are shown in Figure 2 (bottom). The monthly averaged sunspot number and polar field strength derived from magnetograph observations at Wilcox Solar Observatory [http://wso.stanford.edu/Polar.html, *Svalgaard et al.*, 1978; *Hoeksema*, 1995] are also indicated in Figures 2 (top) and 2 (middle), respectively. Polar field data shown here are 20 nHz low-pass filtered values, in which yearly geometric projection effects are eliminated.

The periodic variations in fast and slow wind areas, which are closely associated with the solar cycle, are demonstrated in this figure. Since detailed discussion of this periodic variation between 1985 and 2008 has been presented in *Tokumaru et al.* [2010], we do not repeat it here. However, we discuss here the IPS

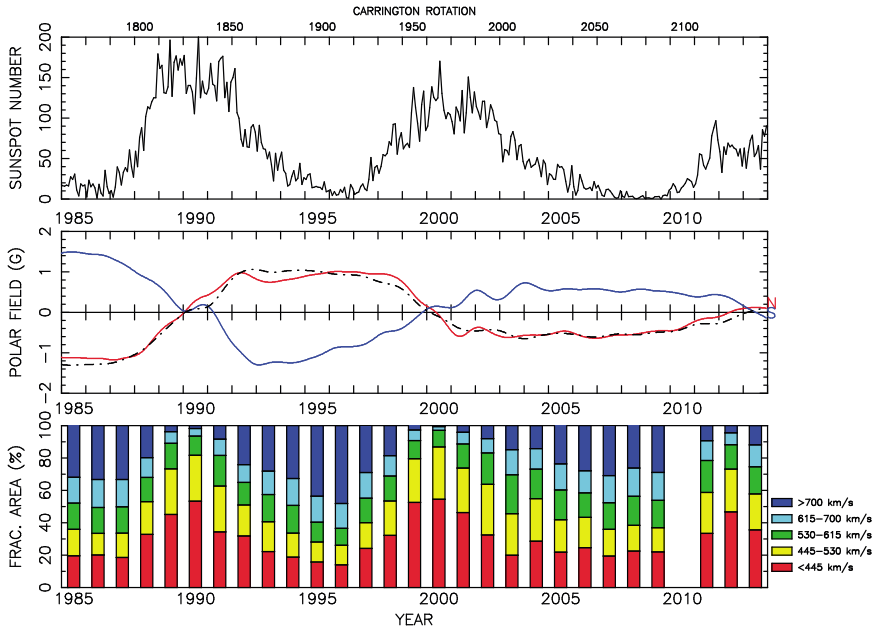

Figure 2. Time variations of (top) monthly mean sunspot numbers, (middle) polar field strength from the Wilcox Solar Observatory, and (bottom) the fractional areas for different solar wind speed ranges at all latitudes during 1985–2013. In Figure 2 (middle), red and blue lines correspond to data at north *N* and south poles *S*, and the dash-dotted line indicates the average value $(N - S)/2$ of polar field strength. In Figure 2 (bottom), red, yellow, green, cyan, and blue correspond to <445 km/s, 445–530 km/s, 530–615 km/s, 615–700 km/s, and >700 km/s, respectively.

observations after 2009. Recent IPS data show that fast (>700 km/s) and slow (<445 km/s) winds reach minimum and maximum areas in 2012, suggesting that Cycle 24 peaked in that year. This fact is generally consistent with polar field data indicating that the polarity reversal has already been completed by 2013. Here one should note the difference in timing of the polarity reversal by 1 year between north and south poles; the polarity at the north pole reversed in 2012, whereas the reversal at the south pole did not occur until 2013. Such a difference in polarity reversal time is also observed in Cycle 23 maximum, and the delay is somewhat smaller than Cycle 24 maximum [*Wang et al.*, 2002; *Svalgaard and Kamide*, 2013].

Figure 3 displays a correlation between polar fields and fractional areas for fast (left) and slow (right) winds. The polar field data are averaged on a yearly basis to compare with the fractional area data. Different symbols are used in the figure to distinguish three intervals corresponding to Cycles 22–24. The correlation coefficients between IPS and polar field data are 0.80 and −0.73 for fast and slow winds, respectively.

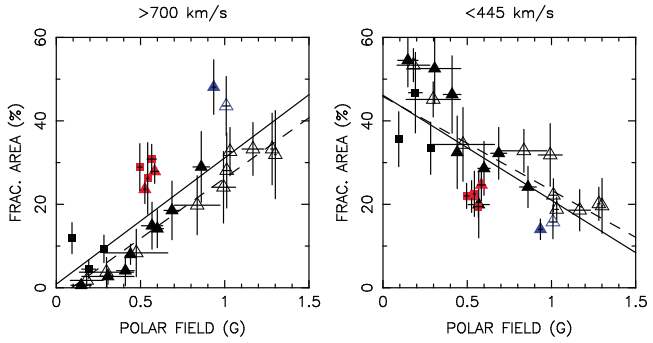

Figure 3. Correlation diagrams between the yearly mean polar field strength and fractional area for (left) >700 km/s and (right) <445 m/s. Open and filled triangles represent data taken during 1985–1995 and 1996–2006, respectively, and filled squares represent those taken during 2007–2013. Blue and red symbols correspond to data at Cycles 22/23 and 23/24 minima, i.e., 1995–1996 and 2005–2009, respectively. Solid and broken oblique lines correspond to linear regression lines for all data and those excluding solar minimum data, respectively. Vertical and horizontal bars represent 2σ values in the mean for a given year.

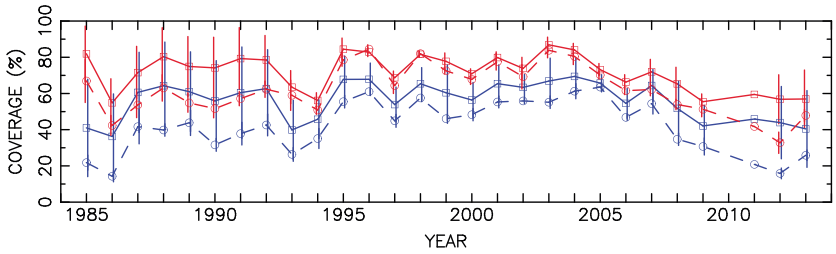

Figure 4. Time variation of areal coverage of STEL observations for north and south latitudes during 1985–2013. Red and blue lines correspond to north and south latitudes, respectively. Solid and dashed lines indicate the coverages for latitude ranges of 0°–90° and 70°–90° in each hemisphere. Vertical bars indicate 2σ values in the mean for a given year.

This close link between polar fields and fast/slow wind areas is explained through the formation of polar coronal holes, i.e., strong polar fields are associated with large coronal holes over the poles, which become a source of fast solar winds. The correlation between the fast wind and the polar field strength is considered more essential than that between the slow wind and the polar field strength, which is considered as a secondary one through balance with the change of the fast wind. Interestingly, the figure reveals that fast wind data taken at Cycles 22/23 and 23/24 minima systematically deviate from the regression line. When we exclude fast wind data at Cycles 22/23 and 23/24 minima, the regression line significantly shifts downward, as indicated by a dashed line in the figure and gives a higher correlation coefficient, 0.93. In the case of the slow wind, the exclusion of IPS data at the solar minima does not yield any significant change in the regression line. The observed deviation of IPS data suggests that more fast winds form at the solar minima than those expected from the linear relation to polar fields. The excess of the fast wind in the minimum period may be ascribed to the effect of higher-order multipole components of the Sun's magnetic field, by which the open field region producing the fast wind tends to form at low latitudes. Except for fast wind data at the solar minima, no systematic difference is found between three intervals corresponding to different cycles (i.e., 1985–1995, 1996–2006, and 2007–2013). Another important point to note here is that the fast (> 700 km/s) wind still forms even for the period of the reduced polar field strength, and this is consistent with Ulysses observations [*McComas et al.*, 2008; *Ebert et al.*, 2013].

4. N-S Asymmetry in Solar Wind Distribution

To investigate the N-S asymmetry in solar wind distribution, we divide our IPS data into two groups in terms of north or south latitude and derive a year-by-year variation of fractional areas corresponding to the different solar wind speed ranges for each hemisphere. Before discussing the result, we must pay attention to the fact that the coverage of our IPS observation is not uniform across latitude and time. The sparse density of lines of sight available for IPS observations results in reduced coverage for the polar solar wind, and the fact that our observation sites are located at geographically north makes the coverage for heliographic south latitudes inferior to that for heliographic north latitudes [see *Tokumaru et al.*, 2010, Figure 2]. Furthermore, the data gaps mentioned above may cause some bias in the IPS data by the effect of nonuniform sampling. Figure 4 demonstrates the coverage of our IPS observations for north and south latitudes during 1985–2013. Here the coverage is defined as a ratio of the source surface area observed by IPS in a given year to the whole area corresponding to 11 solar rotations. As shown here, the southern coverage is systematically smaller than the northern one by 10–20%, and this tendency is nearly unchanged throughout the period analyzed here. The coverage for polar regions drops as compared to that for all latitudes, but there is a difference in this drop between north and south. The drop in the polar coverage at north is much less prominent than that at south, and the polar coverage at north does not significantly differ from the coverage for all latitudes for the period between 1993 and 2006. The drop in the polar coverage at south is usually ~10% but sometimes as large as ~20% for the period of 1985–1992 and 2011–2013. In this study, we use the fractional area which is a ratio of the source surface area corresponding to a given speed range to that observed by IPS, and the effect by the latitude variation in the coverage is considered to be largely suppressed by this normalization. The coverage changes year by year owing to the effect of the data gap, but the change occurs almost simultaneously for both north and south. Therefore, the effect of the data gap is not considered to seriously affect discussion of the N-S asymmetry persisting over a period of ~1 year, although a possibility to miss short-term change cannot be ruled out.

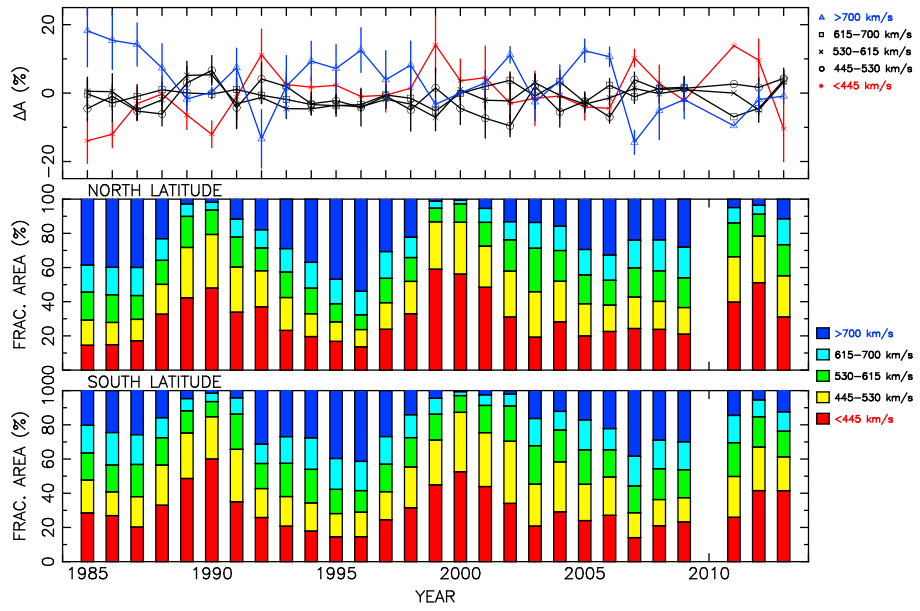

Figure 5. Time variation of (top) difference ΔA between fractional area data of north and south latitudes, and fractional area data in (middle) north and (bottom) south latitudes during 1985–2013. Vertical bars in Figure 5 (top) denote 2σ in the mean for a given year.

The fractional area data for north and south latitudes are shown in Figures 5 (middle) and 5 (bottom), respectively, with the same format as in Figure 3 (bottom). IPS data of north and south latitudes show a similar but slightly different pattern of long-term change. Figure 5 (top) shows the N-S difference ΔA in the fractional area for each speed range. A relatively large ($\sim \pm 10\%$) difference between north and south latitude data sometimes arises for fast and slow speed ranges, while there is no significant N-S difference for intermediate speed ranges. Table 1 shows averages and standard deviations of ΔA for different speed ranges over the whole period. The standard deviations for fast (> 700 km/s) and slow (< 445 km/s) winds are approximately 2 times larger than those for intermediate speed winds. These large standard deviations are ascribed to the occurrence of N-S asymmetry. The mean values of ΔA are smaller than the standard deviations for all speed ranges. This suggests that no significant offset exists throughout the whole period for any speed ranges, while there is pronounced N-S asymmetry of solar winds over the poles as will be described below.

Here we examine robustness of results shown above by using the midpoint data. To do this, we divide IPS data from the time sequence CAT method in terms of the Carrington rotation and calculate the fractional areas corresponding to the five speed groups from a data set for each rotation, then determine a midpoint (i.e., median) value of the fractional areas for a given year. Figure 6 shows the time variation of the factional area produced from the midpoint data for (top) all latitudes, (middle) north, and (bottom) south latitudes, which correspond to Figures 3 (bottom), 5 (middle), and 5 (bottom), respectively. Since the number of Carrington rotations observed in a year is limited, the sum of the midpoint data for the five groups is not necessarily unity. Nevertheless, a quite similar feature to Figures 3 and 5 is revealed in Figure 6, and this fact suggests that the results obtained here are statistically robust.

Figure 7 shows the correlation between polar fields and fast/slow wind areas separately for the respective north and south latitudes. The northern and southern polar field data are averaged on a yearly basis separately. Among meaningful correlations found for all plots, the best one with a coefficient $\rho = 0.80$ is obtained from northern fast wind data. Correlation coefficients are −0.68, 0.65, and −0.65 for northern slow wind, southern fast, and slow winds, respectively. Two regression lines are indicated in each plot, as in

Table 1. Averages and Standard Deviations of ΔA Over the Whole Period

Speed (km/s)	<445	445–530	530–615	615–700	> 700
ΔA (%)	0.03 ± 7.2	-1.4 ± 4	-1.2 ± 3.0	-0.7 ± 2.6	3.3 ± 8.2

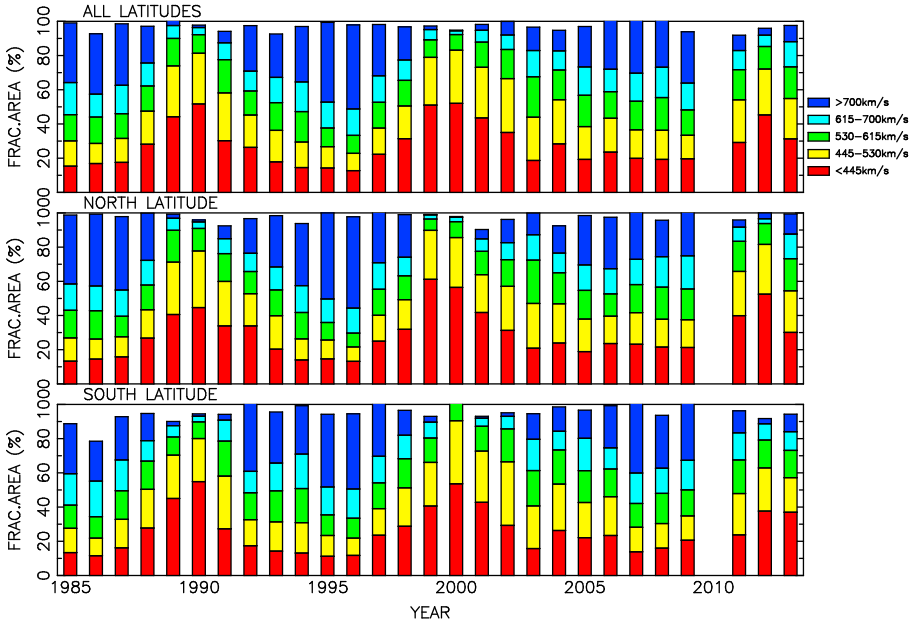

Figure 6. Time variations of midpoint data of the fractional areas for (top) all latitudes, (middle) north, and (bottom) south latitudes and during 1985–2013. The format is the same as that used in Figures 3 (bottom), 5 (middle), and 5 (bottom).

Figure 3. The regression lines for north latitude data exhibit steeper slopes. Systematic deviations from the regression in Cycles 22/23 and 23/24 minima are found for both northern and southern fast wind data, and the regression lines for fast wind data excluding the minimum periods fit better than that for all data.

We examine N-S asymmetry of polar solar winds, since they are sensitive to the solar activity. Figure 8 shows annual variations of fractional areas corresponding to different speed ranges for polar ($|latitude| > 70°$) solar winds between 1985 and 2013. Figures 8 (middle) and 8 (bottom) show IPS data of northern and southern

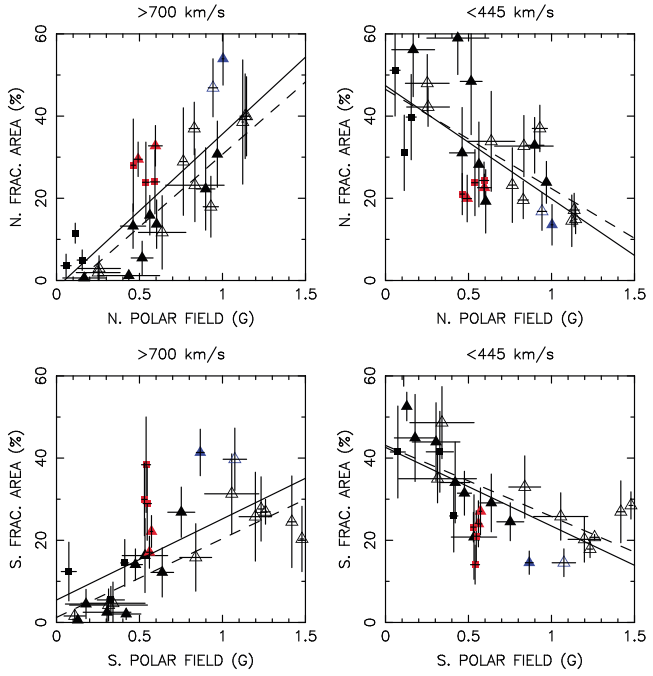

Figure 7. Correlation diagrams between polar field and fractional area of (left) fast and (right) slow winds for (top) north and (bottom) south latitudes. Symbols are the same as those used in Figure 3. Two regression lines are indicated by solid and dashed lines in each plot, as in Figure 3.

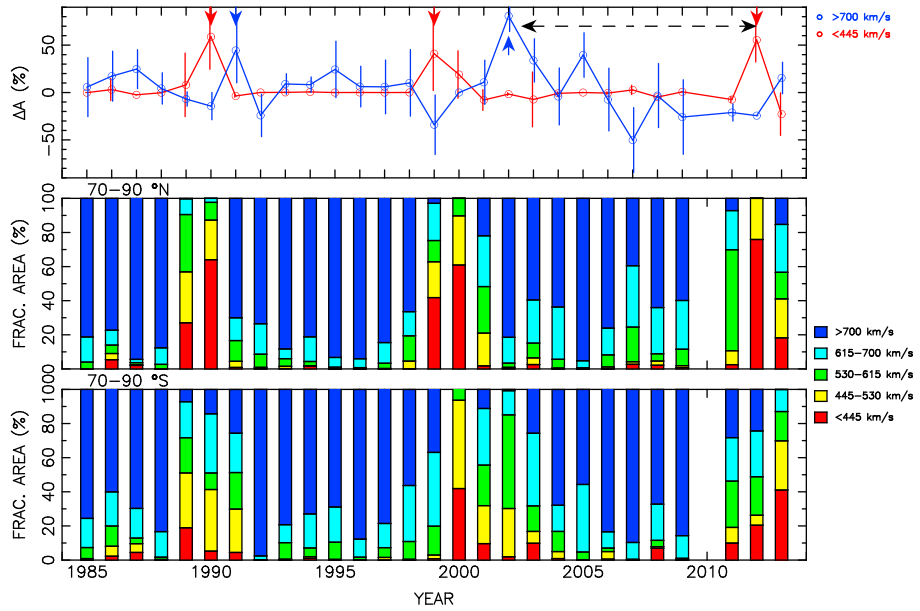

Figure 8. Year-by-year variation of (top) difference ΔA between north and south poles, and fractional area data for (middle) north and (bottom) south poles. In Figure 8 (top), blue and red lines are ΔA for fast and slow winds, respectively, and vertical bars denote 2σ in the mean. As for arrows, refer to the text.

polar solar winds, respectively. Figure 8 (top) shows the N-S difference ΔA for fast and slow winds, and a positive value in the figure represents predominance of the northern wind. As demonstrated here, polar regions are mostly dominated by fast solar wind, and invasion of slow winds to polar regions occurs at solar maxima. Here some interesting features are revealed. First, marked N-S asymmetry in slow wind distribution occurs at solar maxima, and it lasts for about 1 year (as indicated by red arrows in the figure). It should be noted here that the duration of this asymmetry could be shorter than a year, since the analysis is made on yearly basis. We also note that this asymmetry is always shown as a positive peak in Figure 8 (top), i.e., growth of slow winds over the north pole precedes that over the south pole. The precedence of the solar wind evolution over the north pole is consistent with the earlier occurrence of the polarity reversal at the north pole as mentioned in the previous section. Second, N-S asymmetry in fast wind distribution occurs following that in slow wind distribution (as indicated by blue arrows in the figure). Again, the asymmetry is always shown as a positive peak, and this suggests that reformation of fast winds over the north pole occurs earlier than that over the south pole. Third, significant N-S asymmetry of polar fast winds lasts over a long period between the declining phase of Cycle 23 and the maximum of Cycle 24 (as indicated by a horizontal arrow in the figure). This asymmetry starts as a positive peak, i.e., predominance of fast winds over the north pole, following the N-S asymmetry in slow wind distribution at Cycle 23 maximum, and it gradually turns to negative values, showing a peak at Cycle 23/24 minimum. The predominance of fast winds at the south pole continues until Cycle 24 maximum. The observed N-S asymmetry in Cycle 24 is consistent with IPS observations at Ooty, which have reported that the fast wind at the northern region have moved close to the pole but that at the southern region has remained unchanged in the later part of 2011 [*Manoharan*, 2012]. We will compare the observed N-S asymmetry with magnetograph observations in section 6.

Polar fast winds observed for Cycle 23/24 minimum grow smaller than those observed for Cycle 22/23 minimum [*Tokumaru et al.*, 2010; *Manoharan*, 2012; *Ebert et al.*, 2013]. Table 2 shows the fractional areas of north and south polar fast (> 700 km/s) winds averaged over the periods of 1992–1998 and 2003–2009, which correspond to Cycles 22/23 and 23/24 minima, respectively. Our IPS data indicate that a marked reduction in the fractional area (by 18%) occurred for the fast wind over the north pole and also that a relatively moderate reduction (by 10%) occurred for the fast wind over the south pole. The important point to note is that the northern fast wind has a larger fractional area than the southern one during 1992–1998. This fact is consistent with the southward shift of HCS observed for Cycle 22/23 minimum (see section 1). The polar fast wind over the south pole during 2003–2008 has a larger area than the northern one on average, while the difference is small. This small difference does not necessarily mean that the N-S

Table 2. Fractional Areas of North and South Polar Fast (> 700 km/s) Wind for 1992–1998 and 2003–2009

Period	*A* for North Pole	*A* for South Pole
1992–1998	83 ± 9%	77 ± 12%
2003–2009	65 ± 16%	68 ± 21%

asymmetry is small. As mentioned above, ΔA during this period shows a large excursion from a positive value to a negative one, and this results in larger standard deviations of *A* in the mean for both northern and southern polar winds (see Table 2). Therefore, our IPS data suggest the occurrence of significant departure from the symmetric distribution during this period. We note here that the observed N-S asymmetry in the solar wind speed distribution cannot be explained by difference in polar field strength, as will be mentioned in section 6 [see also *Zhang et al.*, 2002].

5. Comparison With Ulysses In Situ Measurements

The N-S asymmetry in polar fast solar winds observed by IPS has been verified by comparing with in situ measurements made by Ulysses (http://omniweb.gsfc.nasa.gov/coho/form/ulysses.html) [*Bame et al.*, 1992]. Figure 9 illustrates the time variation of (Figure 9, top) the solar wind speed measured by Ulysses, and (Figure 9, bottom) its heliographic latitude. The vertical dashed lines indicate the boundaries of periods when Ulysses latitude is between 70° and 80° in north or south. There are six periods of polar scans as shown in Figure 9; S1, N1 in 1994–1995 (first orbit); S2, N2 in 2000–2001 (second orbit); and S3, N3 in 2007–2008 (third orbit). In order to compare with IPS data, we calculate an average speed from Ulysses measurements for each polar scan and the difference in average speeds between north and south scans.

Figure 10 displays (bottom) yearly averages of the solar wind speed measured by our IPS observations for latitude range between 70° and 80° in either north (red) or south (blue), and (top) N-S difference ΔV in the average speed. The N-S asymmetry revealed here has a similar pattern of time variation to that found in the fractional area data for fast winds (Figure 7, top). Ulysses data are also included in this figure. Red and blue short horizontal lines indicated in Figure 10 (bottom) correspond to Ulysses average speeds during north and south polar scans. Black thick horizontal lines in Figure 10 (top) indicate the difference in Ulysses average speeds between north and south polar scans. The N-S difference in Ulysses average speeds during the second orbit is large; 330 km/s, so it is not shown in this figure. Negative and positive peaks of ΔV which occurs at solar maxima mean that the northern polar fast wind disappears and reappears earlier than the

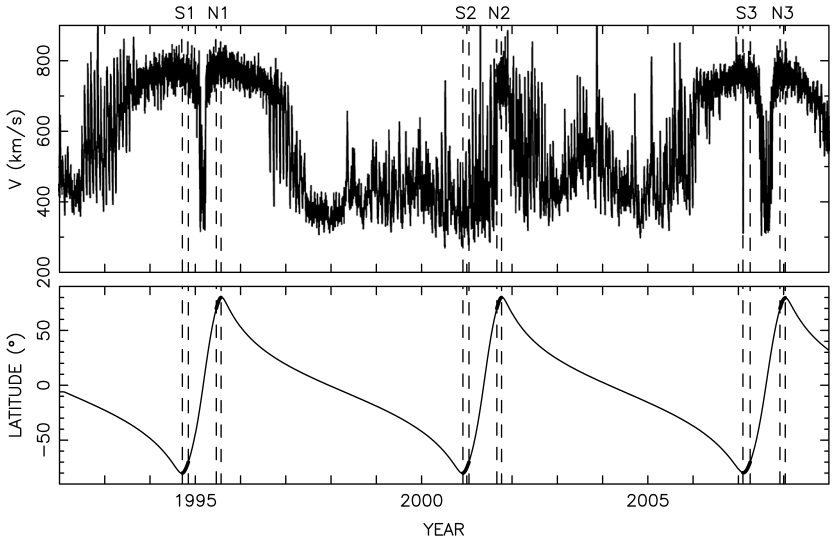

Figure 9. Time variation of (top) hourly averaged solar wind speeds measured by Ulysses, and (bottom) heliographic latitudes of Ulysses during 1992–2008. Vertical dashed lines indicate boundaries at which Ulysses is at 70° north or south. The periods of Ulysses' passages over north or south poles during the first, second, and third orbits are indicated by S1, N1, S2, N2, S3, and N3.

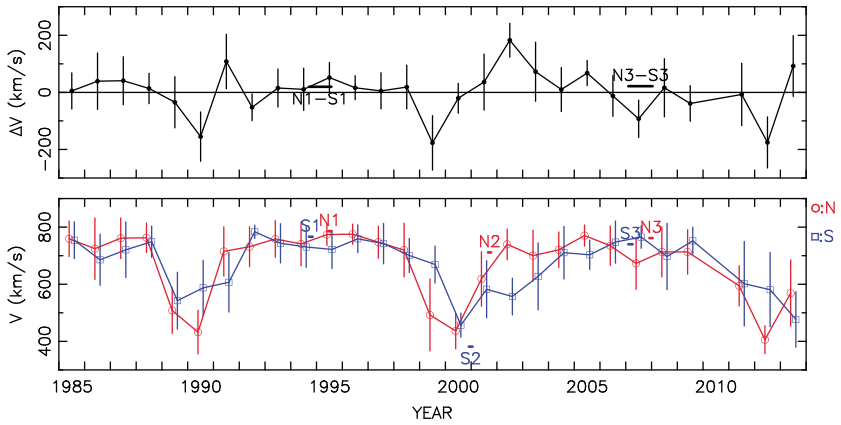

Figure 10. Time variation of (top) difference ΔV between averaged speeds over north and south poles, and (bottom) solar wind speeds averaged over north and south poles, i.e., latitudes between 70° and 80°. In Figure 10 (bottom), red and blue lines are averaged speeds over north and south poles, respectively. Vertical bars are 2σ in the mean of IPS data. Horizontal bars indicate Ulysses data during its polar passages.

southern one. This fact is consistent with the time lag of the polarity reversal observed at the solar maxima. The N-S difference in Ulysses average speeds for the first orbit is 20 km/s, which is consistent with the N-S asymmetry observed by IPS. Here the positive value means that the northern polar wind is faster than the southern one. In the case of the third orbit, Ulysses data suggest that the northern polar wind is 22 km/s faster than the southern one, while IPS data suggest that the southern polar wind is 87 km/s faster. This discrepancy is nearly the same level as the standard deviation, and it could be influenced by temporal variation of the solar wind distribution. Our IPS observations have demonstrated that the solar wind structure was relatively changeable during this period [*Tokumaru et al.*, 2009]. Therefore, we consider that Ulysses data are not too different from IPS data. As for the second orbit, Ulysses data are likely to be greatly affected by temporal variation of the solar wind distribution in the solar maximum of Cycle 23, since it took about 1 year to complete the latitude scan of the second orbit. Since our IPS observations enable to determine the latitude profile of the solar wind speed in a shorter time, i.e., nearly one solar rotation period, we consider that the effect is less significant than Ulysses data. However, the IPS data given on a yearly basis are still likely to fail to accurately identify short-lived features, and the occurrence of the data gap is thought to increase this misidentification. Nevertheless, as demonstrated in Figure 10 (bottom), the Ulysses average speeds for the second orbit (blue and red horizontal bars) are roughly consistent with the IPS average speeds (blue and red lines). We also have found that speeds derived from IPS along the Ulysses trajectory in 2001 (the second

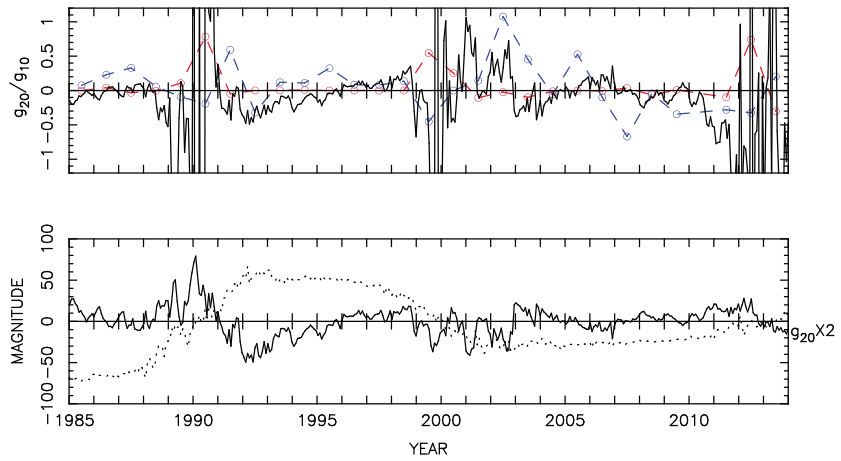

Figure 11. Time variation of (top) $g20/g10$ and ΔA, and (bottom) $g20$ and $g10$ from Wilcox Solar Observatory. In Figure 11 (top), solid line denotes $g20/g10$ and blue and red broken lines are ΔA for fast and slow winds, respectively. In Figure 11 (bottom), solid and dotted lines are $g20$ and $g10$. The value of $g20$ is magnified 2 times.

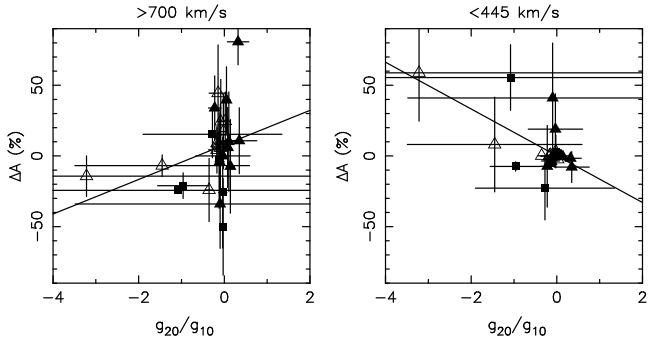

Figure 12. Correlation diagram between $g20/g10$ and ΔA for (left) > 700 km/s and (right) < 445 km/s. The oblique lines are the linear regression lines. Symbols are the same as those used in Figure 3.

orbit) are in good agreement with those measured by Ulysses [*Fujiki et al.*, 2003]. Hence, we consider that Ulysses data are generally consistent with IPS observations.

6. Comparison With Solar Magnetic Field Properties

The N-S asymmetry of polar fast winds is considered to originate from properties of the Sun's magnetic field. In this study, we examine the relation between the N-S asymmetry of polar fast winds and the quadrupole component of the Sun's magnetic field. The field represented by the quadrupole has the same polarity at both poles, so that it may give rise to N-S asymmetry if combined with the dipole field. The quadrupole term of the solar magnetic field was proposed as a possible cause for the N-S asymmetry of the heliosphere [*Bravo and Gonzalez-Esperza*, 2000; *Wang and Robbrecht*, 2011]. Since the dipole field weakens in this cycle, the relative importance of the quadrupole component should increase. The enhanced N-S asymmetry of polar fast winds after Cycle 23 maximum may be explained by this effect. Here it should be noted that our IPS data may be influenced by the effect of the data gap, as mentioned in sections 4 and 5.

Figure 11 indicates the time variation of (bottom) harmonic coefficients g_{10} (dotted line) and g_{20} (solid line, magnified 2 times), and (Figure 11, top) the ratio g_{20}/g_{10} during 1985–2013. The coefficients g_{10} and g_{20} correspond to the magnitudes of the axial dipole ($l = 1$, $m = 0$) and the axis-asymmetric quadrupole ($l = 2$, $m = 0$) components in a spherical harmonic series of the scalar magnetic field potential. In this study, we use data of g_{10} and g_{20} obtained from the potential field analysis made at the Wilcox Solar Observatory (http://wso.stanford.edu/Harmonic.los/ghlist.html) [*Zhao and Hoeksema*, 1993]. During solar maxima, the ratio g_{20}/g_{10} shows prominent displacements from zero, since g_{10} becomes small. These displacements tend

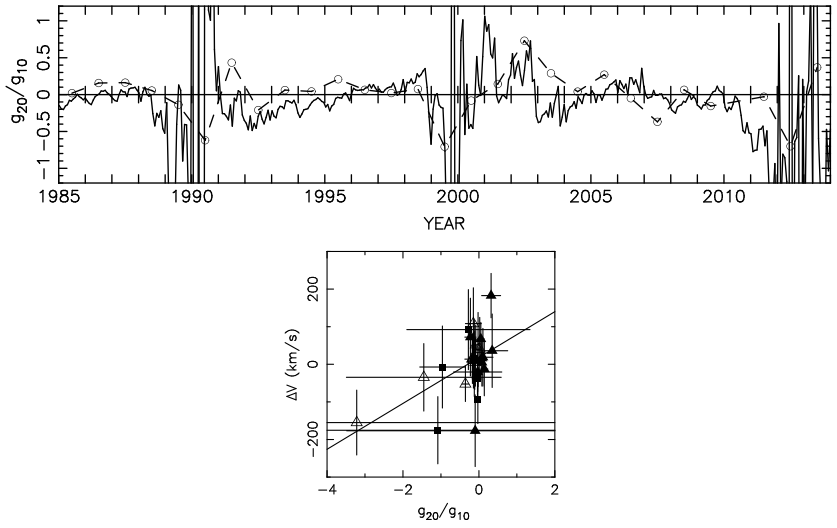

Figure 13. (top) Time variation of $g20/g10$ (solid line) and ΔV (broken line), and (bottom) correlation diagram between $g20/g10$ and ΔV.The oblique line corresponds to the linear regression line.

Table 3. Correlation Coefficients Between Wilcox Solar Observatory and IPS Data

	ΔA (> 700 km/s)	ΔA (< 445 km/s)	ΔV
g_{20}/g_{10}	0.32	−0.64	0.53
g_{20}	−0.19	0.33	−0.28
ΔB	0.09	0.04	0.04

to show a positive value of g_{20}/g_{10} immediately after the solar maxima and a negative value before the solar maxima. We note that the displacement after Cycle 23 maximum and that before Cycle 24 maximum last longer than those after Cycle 22 maximum and before 23 maximum. In Figure 11 (top), the ΔA for polar fast and slow winds (see Figure 7, top) are plotted by dashed lines. The large displacement of g_{20}/g_{10} appears similar with time variation of N-S asymmetry of polar solar winds. The correlation diagrams between g_{20}/g_{10} and ΔA are shown in Figure 12 for polar fast (> 700 km/s) and slow (< 445 km/s) winds. Here we calculate an average ratio of g_{20}/g_{10} for each year to compare with IPS data. Since g_{10} becomes nearly zero at solar maxima, g_{20}/g_{10} exhibits a large fluctuation and this results in large RMS bars in the figure. A moderate degree of negative correlation with $\rho = -0.64$ is revealed from comparison between g_{20}/g_{10} and polar slow wind ΔA, whereas the correlation between g_{20}/g_{10} and polar fast wind ΔA is poor, $\rho = 0.32$. The corresponding level of significance of the null hypothesis for these correlations are 0.00025 and 0.096, respectively. Therefore, the null hypothesis is safely rejected for the case of polar slow wind when the confidence level of 95% is used. For the case of polar fast wind, the null hypothesis cannot be ruled out, since $0.096 > 0.05 = 1-0.95$. Here we should notice that some data which are crucial for yielding a meaningful correlation have large standard deviations, so that the result obtained here may have some uncertainty.

Another meaningful correlation is revealed from the comparison between g_{20}/g_{10} and ΔV data. Figure 13 (top) shows the time variation of g_{20}/g_{10} and ΔV (see Figure 10, top) during 1985–2013, and (Figure 13, bottom) the correlation between them. A moderate degree of correlation with $\rho = 0.53$ is revealed here. The corresponding level of significance of the null hypothesis is 0.0037 for this correlation, so that the null hypothesis is safely rejected for this case. Table 3 shows the correlation coefficients for the cases of comparison with $g_{20}/_{10}$, g_{20}, and ΔB, which is the difference between magnetic field strengths at north and south poles (see Figure 3, middle). As shown here, the correlation coefficients greatly degrade when IPS data are compared with g_{20} directly, and no meaningful correlation is found for the comparison between IPS data and ΔB. We note again that some data have large standard deviations which may affect the result significantly.

7. Summary and Conclusions

STEL IPS observations are analyzed to study the N-S asymmetry in global distribution of the solar wind speed between 1985 and 2013. As result, we obtain the following results:

1. Global distribution of the solar wind speed is found to change systematically with the solar dynamo activity. Our IPS data suggest that fast winds in Cycle 23/24 minimum grow smaller than those in Cycle 22/23 minimum. Northern fast winds during Cycle 22/23 minimum are found to have a larger area than southern ones, and this is consistent with the southward shift of HCS reported from earlier studies and also consistent with Ulysses and Ooty IPS observations [*Ebert et al.*, 2013; *Manoharan*, 2012].
2. Fast and slow wind areas on the source surface show good positive and negative correlations with polar fields, respectively. The IPS data taken in Cycles 22/23 and 23/24 minima appear to deviate from a linear relation between polar fields and solar winds, indicating that more fast winds are formed in those periods than expected from polar fields. As polar fields in this cycle weaken, higher-order multipole components of the Sun's magnetic field may contribute more importantly to formation of open flux regions, which generate fast winds. Such nondipolar fields tend to form open flux regions at low latitudes, consistent with the increase in the fast wind area at low latitudes in Cycle 24 [*Tokumaru et al.*, 2009, 2010]. However, deviation from the regression line is also observed in Cycle 22/23 minimum, when the dipole component is dominant. Therefore, all of the observed deviations cannot be ascribed to the effect of higher-order multipole components.
3. A similar but significantly different pattern of the solar cycle change is found in the solar wind distribution for northern and southern hemispheres. A better correlation between polar fields and solar winds is

observed for the northern hemisphere, and the highest one is between polar fields and northern fast winds. We consider that the better correlation found for northern hemisphere is likely to be intrinsic, since solar radio observations at 17 GHz during 1992–2013, which serve as an excellent indicator of the solar activity, show that the radio brightness at low and high latitudes is strongly anticorrelated in the northern hemisphere, whereas this anticorrelation is weak in the southern hemisphere [*Shibasaki*, 2013]. While the cause for weakening of the synchronization between high and low latitude activities in the southern hemisphere is not understood yet, it may provide an important insight into long-term properties of the dynamo process. Poorer correlation between polar fields and solar wind distribution for the southern hemisphere may be interpreted in a similar way.

4. Significant N-S asymmetry is found for polar solar winds, particularly in the solar maximum. The growth of slow winds over the north pole always occurs earlier than that over the south pole at solar maxima. This N-S asymmetry of polar slow winds lasts for about 1 year and followed by that of polar fast winds. As with slow winds, northern polar fast winds reform earlier than southern ones. Our finding is consistent with earlier polarity reversal of the north pole at the solar maxima reported from magnetograph observations at Mount Wilson Observatory [*Svalgaard and Kamide*, 2013]. Polar fast winds exhibit enhanced N-S asymmetry for a long period, starting with an excess of northern fast winds just after Cycle 23 maximum and ending with that of southern fast winds before Cycle 24 maximum. The enhancement of the N-S asymmetry observed after Cycle 23 maximum may be interpreted as due to the effect of higher-order multipole components.
5. The N-S asymmetry of polar solar winds revealed from our IPS observations is found to be generally consistent with the N-S difference observed by Ulysses. It should be noted that the latitude range used here to investigate the polar solar wind is $> 70°$. Ulysses measurements have indicated that the polar solar wind at $> |60°|$ was less variable and rather uniform [*Ebert et al.*, 2013]. Our results suggest that there exist some variability and asymmetry associated with the solar activity even in this latitude range. More variable fast wind, which is considered as a main driver of the hemispheric differences in several parameters of the solar wind and IMF, has been identified between 40°S and 60°S from Ulysses measurements. Detailed analysis of this variable fast wind using IPS observations is an interesting future subject.
6. A moderate degree of meaningful correlation is found between the N-S asymmetry of solar wind speed over the poles and the ratio g_{20}/g_{10}. No significant correlation is found between the N-S asymmetry of polar solar wind speed (IPS data) and g_{20} data and also between IPS and ΔB data. This suggests that higher-order multipole moments such as the quadrupole play an important role in forming the asymmetric distribution of the solar wind. However, it is premature to conclude that the quadrupole is a key factor causing observed asymmetry, partly since the correlation is not very high and partly since there are other important factors for solar wind acceleration such as the flux tube expansion rate [*Wang and Sheeley*, 1990; *Hakamada et al.*, 2002]. Therefore, we must pursue the origin of the solar wind asymmetry further in a future study.

Acknowledgments

The IPS observations have been carried out under the solar wind program of the Solar-Terrestrial Environment Laboratory (STEL) of Nagoya University. This work was supported by a grant-in-aid for Scientific Research (A) (25247079) and by the IUGONET project of MEXT, Japan. We would like to thank the Wilcox Solar Observatory (WSO) for providing open access to the magnetograph data. We also would like to acknowledge use of NSSDC COHO web archives for Ulysses data. We would like to thank Masayoshi Kojima for his useful comments. The STEL IPS observations are available from http://stsw1.stelab.nagoya-u.ac.jp/ips_data-e.html. The WSO and Ulysses observations were obtained from http://wso.stanford.edu/ and http://omniweb.gsfc.nasa.gov/coho/, respectively.

Yuming Wang thanks P.K. Manoharan and another reviewer for their assistance in evaluating this paper.

References

Asai, K., Y. Ishida, M. Kojima, K. Maruyama, H. Misawa, and N. Yoshimi (1995), Multi-station system for solar wind observations using the interplanetary scintillation method, *J. Geomagn. Geoelec.*, *47*, 1107–1112.

Asai, K., M. Kojima, M. Tokumaru, A. Yokobe, B. V. Jackson, P. L. Hick, and P. K. Manoharan (1998), Heliospheric tomography using interplanetary scintillation observations. III. Velocity dependence of electron density fluctuations, *J. Geophys. Res.*, *103*, 1991–2001.

Bame, S. J., D. J. McComas, B. L. Barraclough, J. L. Phillips, K. J. Sofaly, J. C. Chavez, B. E. Goldstein, and R. K. Sakurai (1992), The Ulysses solar wind plasma experiment, *Astron. Astrophys. Suppl.*, *92*, 237–266.

Bravo, S., and J. A. Gonzalez-Esperza (2000), The north-south asymmetry of the solar and heliospheric magnetic field during activity minima, *Geophys. Res. Lett.*, *27*(6), 847–849.

Bzowski, M., T. Makinen, E. Kyrola, T. Summanen, and E. Quemerais (2003), Latitudinal structure and north-south asymmetry of the solar wind from Lyman-α remote sensing by SWAN, *Astron. Astrophys.*, *408*, 1165–1177.

Chowdhury, P., D. P. Choudhary, and S. Gosain (2013), A study of the hemispheric asymmetry of sunspot area during solar cycles 23 and 24, *Astrophys. J.*, *768*, 188, doi:10.1088/0004-637X/768/2/188.

Coles, W. A., B. J. Rickett, V. H. Rumsey, J. J. Kaufman, D. G. Turley, S. Ananthakrishnan, J. W. Armstrong, J. K. Harmon, S. L. Scott, and D. G. Sime (1980), Solar cycle changes in the polar solar wind, *Nature*, *286*, 239–241.

Cowling, T. G. (1933), The magnetic field of sunspots, *Mon. Not. R. Astron. Soc.*, *94*, 39–48.

Ebert, R. W., M. A. Dayeh, M. I. Desai, D. J. McComas, and P. N. Pogorelov (2013), Hemispheric asymmetries in the polar solar wind observed by Ulysses near the minima of solar cycles 22 and 23, *Astrophys. J.*, *768*, 160, doi:10.1088/0004-637X/768/2/160.

Erdos, G., and A. Balogh (2010), North-south asymmetry of the location of the heliospheric current sheet revisited, *J. Geophys. Res.*, *115*, A01105, doi:10.1029/2009JA014620.

Fujiki, K., M. Kojima, M. Tokumaru, T. Ohmi, A. Yokobe, K. Hayashi, D. J. McComas, and H. A. Elliott (2003), How did the solar wind structure change around the solar maximum? From interplanetary scintillation observation, *Ann. Geophys.*, *21*, 1257–1261.

Hakamada, K., M. Kojima, M. Tokumaru, T. Ohmi, A. Yokobe, and K. Fujiki (2002), Solar wind speed and expansion rate of the coronal magnetic field in solar maximum and minimum phases, *Sol. Phys.*, *207*, 173–185.

Hoeksema, J. T. (1995), The large-scale structure of the heliospheric current sheet during the ULYSSES epoch, *Space Sci. Rev.*, *72*, 137–148.

Kojima, M., and T. Kakinuma (1990), Solar cycle dependence of global distribution of solar wind speed, *Space Sci. Rev.*, *53*, 173–222.

Kojima, M., M. Tokumaru, H. Watanabe, A. Yokobe, K. Asai, B. V. Jackson, and P. L. Hick (1998), Heliospheric tomography using interplanetary scintillation observations. II. Latitude and heliocentric distance dependence of solar wind structure at 0.1–1 AU, *J. Geophys. Res.*, *103*, 1981–1989.

Kojima, M., K. Fujiki, T. Ohmi, M. Tokumaru, A. Yokobe, and K. Hakamada (2001), Latitudinal velocity structures up to the solar poles estimated from interplanetary scintillation tomography analysis, *J. Geophys. Res.*, *106*(A8), 15,677–15,686.

Kojima, M., M. Tokumaru, K. Fujiki, K. Hayashi, and B. V. Jackson (2007), IPS tomographic observations of 3D solar wind structure, *Astron. Astrophys. Trans.*, *26*(6), 467–476.

Jackson, B. V., P. P. Hick, M. Kojima, and A. Yokobe (1998), Heliospheric tomography using interplanetary scintillation observations: I. Combined Nagoya and Cambridge data, *J. Geophys. Res.*, *103*, 12,049–12,067.

Jian, L. K., C. T. Russell, and J. G. Luhmann (2011), Comparing solar minimum 23/24 with historical solar wind records at 1 AU, *Sol. Phys.*, *274*, 321–344, doi:10.1007/s11207-011-9737-2.

Manoharan, P. K. (2012), Three-dimensional evolution of solar wind during solar cycles 22–24, *Astrophys. J.*, *751*, 128, doi:10.1088/0004-637X/751/2/128.

McComas, D. J., B. L. Barraclough, H. O. Funsten, J. T. Gosling, E. Snatiago-Muñoz, R. M. Skoug, B. E. Goldstein, M. Neugebauer, P. Riley, and A. Balogh (2000), Solar wind observations over Ulysses' first full polar orbit, *J. Geophys. Res.*, *105*, 10,419–10,433, doi:10.1029/1999JA000383.

McComas, D. J., R. W. Ebert, H. A. Elliott, B. E. Goldstain, J. T. Gosling, N. A. Schwadron, and R. M. Skoug (2008), Weaker solar wind from the polar coronal holes and the whole Sun, *Geophys. Res. Lett.*, *35*, L18103, doi:10.1029/2008GL034896.

McComas, D. J., N. Angold, H. A. Elliott, G. Livadiotis, N. A. Schwadron, R. M. Skoug, and C. W. Smith (2013), Weakest solar wind of the space age and the current "mini" solar maximum, *Astrophys. J.*, *799*, 2, doi:10.1088/0004-637X/779/1/2.

Rosenberg, R. L. (1975), Heliographic latitude dependence of the IMF dominant polarity in 1972–1973 using Pioneer 10 data, *J. Geophys. Res.*, *80*(10), 1339–1340.

Shibasaki, K. (2013), Long-term global solar activity observed by the Nobeyama Radioheliograph, *Publ. Astron. Soc. Jpn.*, *65*, S17.

Simpson, J. A., M. Zhang, and S. Bame (1996), A solar polar north-south asymmetry for cosmic-ray propagation in the heliosphere: The Ulysses pole-to-pole rapid transit, *Astrophys. J.*, *465*, L69–L72.

Smith, E. J., A. Balogh, M. E. Burton, R. Forsyth, and R. P. Lepping (1997), Radial and azimuthal components of the heliospheric magnetic field: Ulysses observations, *Adv. Space Res.*, *20*(1), 47–53.

Smith, E. J., J. R. Jokipii, J. Kota, R. P. Lepping, and A. Szabo (2000), Evidence of a north-south asymmetry in the heliosphere associated with a southward displacement of the heliospheric current sheet, *Astrophys. J.*, *533*, 1084–1089.

Svalgaard, L., and Y. Kamide (2013), Asymmetric solar polar field reversals, *Astrophys. J.*, *763*, 23, doi:10.1088/00004-637X/763/1/23.

Svalgaard, L., T. L. Duvall Jr., and P. H. Scherrer (1978), The Strength of the Sun's polar fields, *Sol. Phys.*, *58*, 225–240.

Tokumaru, M. (2013), Three-dimensional exploration of the solar wind using observations of interplanetary scintillation, *Proc. Jpn. Acad. B*, *89*(2), 67–79.

Tokumaru, M., M. Kojima, Y. Ishida, A. Yokobe, and T. Ohmi (2000), Large-scale structure of solar wind turbulence near the solar activity minimum, *Adv. Space Res.*, *25*(9), 1943–1946.

Tokumaru, M., M. Kojima, K. Fujiki, and K. Hayashi (2009), Non-dipolar solar wind structure observed in the cycle 23/24 minimum, *Geophys. Res. Lett.*, *36*, L09101, doi:10.1029/2009GL037461.

Tokumaru, M., M. Kojima, and K. Fujiki (2010), Solar cycle evolution of the solar wind speed distribution from 1985 to 2008, *J. Geophys. Res.*, *115*, A04102, doi:10.1029/2009JA014628.

Tokumaru, M., M. Kojima, K. Fujiki, M. Maruyama, Y. Maruyama, H. Ito, and T. Iju (2011), A newly developed UHF radiotelescope for interplanetary scintillation observations: Solar wind imaging facility, *Radio Sci.*, *46*, RS0F02, doi:10.1029/2011RS004694.

Tokumaru, M., M. Kojima, and K. Fujiki (2012), Long-term evolution in the global distribution of solar wind speed and density fluctuations for 1997–2009, *J. Geophys. Res.*, *117*, A06108, doi:10.1029/2011JA017379.

Tritakis, V. P. (1984), Heliospheric current sheet displacements during the solar cycle evolution, *J. Geophys. Res.*, *89*(A8), 6588–6598.

Virtanen, I. I., and K. Mursla (2010), Asymmetry of solar polar fields and the southward shift of HCS observed by Ulysses, *J. Geophys. Res.*, *115*, A09110, doi:10.1029/2010JA015275.

Wang, Y. -M., and E. Robbrecht (2011), Asymmetric sunspot activity and the southward displacement of the heliospheric current sheet, *Astrophys. J.*, *736*, 136, doi:10.1088/0004-637X/736/2/136.

Wang, Y. -M., and N. R. Sheeley (1990), Solar wind speed and coronal flux-tube expansion, *Astrophys. J.*, *355*, 726–733.

Wang, Y. -M., N. R. Sheeley, and M. D. Andrews (2002), Polarity reversal of the solar magnetic field during cycle 23, *J. Geophys. Res.*, *107*(A12), 1465, doi:10.1029/2002JA009463.

Zhang, J., J. Woch, S. K. Solanki, and R. von Steiger (2002), The Sun at solar minimum: North-South asymmetry of the polar coronal holes, *Geophys. Res. Lett.*, *29*(8), 1236, doi:10.1029/2001GL014471.

Zhao, X. P., and J. T. Hoeksema (1993), Unique determination of model coronal magnetic fields using photospheric observations, *Sol. Phys.*, *143*, 41–48.

Zhao, X. P., J. T. Hoeksema, and P. H. Scherrer (2005), Prediction and understanding of the north-south displacement of the heliospheric current sheet, *J. Geophys. Res.*, *110*, A10101, doi:10.1029/2004JA010723.